https://doi.org/10.5194/egusphere-2026-3287
Preprint. Discussion started: 24 June 2026

Tracking spatiotemporally contiguous heatwave hazards over mainland China: persistence, severity, spatial extent, and mobility

Hao Guo[1,2], Qinghou Hang[1,2], Xiangchen Meng[1,2], Ye Yuan[3], Ying Cao[1,2], Yunqian Wang[1,2], Philippe De Maeyer[4,5]

[1]School of Geography and Tourism, Qufu Normal University, Rizhao 276826, China
[2]Sino-Belgian Joint Laboratory for Geo-Information, Rizhao 276826, China
[3]Xinjiang Institute of Ecology and Geography, Chinese Academy of Sciences, Urumqi, 830011, China
[4]Department of Geography, Ghent University, Gent, 9000, Belgium
[5]Sino-Belgian Joint Laboratory for Geo-Information, Gent, 9000, Belgium.

Correspondence to: Hao Guo (guohao@qfnu.edu.cn)

Abstract. Under continued warming, heatwaves increasingly evolve as regional processes that persist, expand, and migrate across space. Using ERA5-Land daily maximum temperature data, we identified spatiotemporally contiguous heatwave events over mainland China during May–September of 1986–2024 and quantified their persistence, severity, affected area, and mobility. The study period was divided into three phases according to changes in annual mean daily maximum temperature: 1986–1998, 1999–2011, and 2012–2024. A total of 609 events were identified, including 177, 219, and 213 events in the three phases, respectively. Although event number did not continue to increase after 2012, event characteristics intensified markedly. During 2012–2024, the fitted rates of change in duration, cumulative severity, affected area, and track length reached 0.264 days yr^{-1}, 2.6 × 10^6 °C days km^2 yr^{-1}, 1.0 × 10^5 km^2 yr^{-1}, and 116.06 km yr^{-1}, respectively. Track length was significantly correlated with duration, severity, and affected area, and these relationships were strongest after 2012. The results indicate that recent heatwave hazards in mainland China are characterized mainly by stronger contiguous event processes rather than by more frequent events.

1 Introduction

Heatwaves (HWs) are among the most consequential atmospheric extremes in a warming climate, with widespread impacts on human health, ecosystem functioning, agricultural production, and energy systems (Perkins-Kirkpatrick and Lewis, 2020; Wu et al., 2025; Bell et al., 2024). Over recent decades, many regions of the world have experienced an increase in heatwave frequency, duration, and intensity, indicating that heatwave risk is evolving from localized short-term exposure toward broader and more persistent regional impacts (Martinez-Villalobos et al., 2025; Wang et al., 2024a; Perkins-Kirkpatrick and Lewis, 2020). However, heatwaves are not simply sets of hot days occurring independently at fixed locations. Under the joint influence of large-scale atmospheric circulation and land-surface thermal conditions, they often develop as continuous regional processes that persist, expand, migrate, and decay through space and time (Horowitz et al., 2022; Skinner et al.,

https://doi.org/10.5194/egusphere-2026-3287
Preprint. Discussion started: 24 June 2026

2025; Wang et al., 2025). A process-based understanding of heatwaves therefore requires attention not only to how often they occur, but also to how their spatiotemporal structure evolves under continued warming.

The way heatwaves are identified largely determines which characteristics of their evolution can be observed (Martinez-Villalobos et al., 2025). Previous studies have widely employed methods such as relative threshold approaches (Perkins-Kirkpatrick and Lewis, 2020; Qiu and Yan, 2020), run theory (Yao et al., 2022; Zhou et al., 2024; Hobday et al., 2016), empirical orthogonal function (EOF) analysis (Buschow et al., 2024; Yu et al., 2021), wavelet analysis (Enliang et al., 2020), as well as principal component analysis and cluster analysis (Yang et al., 2024; Chauhan et al., 2023; Happé et al., 2024) to identify heatwaves and quantify their frequency, duration, and intensity at grid-cell or station scales. These studies have provided an important foundation for understanding heatwave variability. Nevertheless, most of them still treat heatwaves either as persistent hot episodes in local time series or as spatial patterns confined to a specific period. Such lower-dimensional perspectives are useful for describing where and when heatwaves occur, but they are less effective for preserving the continuity of regional heatwave processes, especially when events evolve across regions, undergo marked spatial expansion, or exhibit clear migration pathways (Hu et al., 2023; Al-Yaari et al., 2023; White et al., 2023). For heatwaves that evolve across regions, expand continuously, and exhibit pronounced spatial migration, such dimensional reduction can easily lead to the loss of information on migration pathways, dynamic changes in affected extent, and spatial continuity (Luo et al., 2022b; Zhang et al., 2025).

In addition to duration and cumulative heat load, heatwaves also possess dynamic properties such as movement direction, migration distance, and spatial expansion and contraction, all of which directly influence the affected extent of an event and the way in which it evolves (Luo et al., 2024). For example, Dar and Apurv (2024) found that pre-monsoon heatwaves in India can migrate from the northwest toward the northeast or southeast, while continuously expanding their spatial extent during the course of evolution.

To address this limitation, increasing attention has been given to heatwaves as contiguous spatiotemporal events in a three-dimensional longitude-latitude-time framework. Sánchez-Benítez et al. (2018) defined heatwaves as continuous clusters in three-dimensional space, providing a basis for event-oriented analyses. Building on this perspective, Luo et al. (2022c) characterized continuous heatwaves in China in terms of duration, intensity, centroid location, and movement direction, while Ren et al. (2025) further employed a three-dimensional DBSCAN framework to analyse multidimensional heatwave characteristics. Recent studies have also shown that migrating heatwaves can become more prominent under climate warming and may reflect preferred migration pathways at regional to continental scales (Gu et al., 2025; Wang et al., 2025; Skinner et al., 2025; Horowitz et al., 2022). Together, these studies demonstrate that the three-dimensional event-based perspective can capture aspects of heatwave evolution that are difficult to resolve using conventional grid-based or regional-average approaches.

Despite this progress, several important questions remain insufficiently addressed. Existing three-dimensional studies have focused mainly on the overall spatiotemporal characteristics, migration patterns, or long-term changes of heatwaves, whereas less attention has been paid to whether key event characteristics undergo phase-dependent transitions under rapid warming.

https://doi.org/10.5194/egusphere-2026-3287
Preprint. Discussion started: 24 June 2026

In particular, it remains unclear whether persistence, cumulative severity, affected area, and mobility intensify jointly during the recent rapid-warming phase, or whether stronger mobility is systematically associated with longer duration, greater cumulative heat stress, and broader spatial extent. In addition, the extent to which these relationships vary within the warm season has not been fully examined. These issues matter because, if recent heatwave change is expressed mainly through the strengthening of event processes rather than through a simple increase in event counts, then the risk implications of heatwaves may also need to be reconsidered from a process-based perspective.

Mainland China provides an important setting for addressing these questions. It spans a wide range of climatic regimes and topographic conditions, and it has experienced pronounced warming as well as substantial socioeconomic and ecological exposure to heat extremes (Luo et al., 2024; Jiang et al., 2024; Feng et al., 2025; Cai et al., 2021; Lyu et al., 2025). For example, Cai et al. (2021) reported that heatwave-related impacts were associated with approximately 26,800 deaths in China in 2019, and that the mortality burden had continued to increase, rising by about 1,000 deaths every 1.2 years on average. Heatwave impacts in China are not limited to human health. Xu et al. (2024) showed that the record-breaking heatwave of summer 2022 suppressed vegetation growth across more than half of the country's vegetated areas, leading to a marked decline in vegetation productivity. At the same time, the large spatial gradients in climate and terrain across mainland China make it especially suitable for investigating how contiguous heatwave events evolve, migrate, and intensify across different warming phases.

Against this background, this study examines heatwaves over mainland China during May-September of 1986–2024 as contiguous three-dimensional events using ERA5-Land daily maximum temperature data. The study period is first divided into three warming phases according to variations in annual mean daily maximum temperature. Heatwave events are then identified within a longitude-latitude-time framework, and their key characteristics, including frequency, duration, cumulative severity, affected area, migration distance, and moving speed, are compared across phases. On this basis, the relationships between mobility and other event characteristics are evaluated, intra-seasonal differences are examined, and representative events are used to illustrate phase-dependent contrasts in process evolution. By doing so, this study aims to clarify whether recent heatwave change over mainland China is characterized primarily by increasing event numbers or by the joint intensification of multiple event characteristics and whether migration distance has particular process significance in understanding contiguous heatwave evolution under rapid warming.

2 Datasets and methods

2.1 Study Area

The study area of this research is mainland China, located in eastern Eurasia, extending approximately from 3°51′N to 53°33′N and from 73°33′E to 135°05′E, with a land area of about 9.6 million km² (Qiao et al., 2024; Tian et al., 2025) (Figure 1a). Mainland China is characterized by complex topography and a three-step terrain pattern that generally descends from west to east, transitioning from the Qinghai-Tibet Plateau and its surrounding mountains and plateaus to the plains and

https://doi.org/10.5194/egusphere-2026-3287
Preprint. Discussion started: 24 June 2026

hills of central and eastern China (Figure 1b), thereby forming pronounced topographic gradients and diverse climatic types (Shi et al., 2024a; Li et al., 2025). As a result, the spatial variation in temperature across mainland China is substantial, with lower annual mean maximum temperatures in plateau and mountainous regions and higher values in the plains and hilly areas of central and eastern China (Figure 1c). At the seasonal scale, the mean maximum temperature from May to September exhibits a unimodal pattern, peaking in July and remaining relatively lower in May and September, indicating clear intra-seasonal variation during the warm season. The complex topographic conditions, pronounced spatial temperature gradients, and distinct month-to-month variation during the warm season together make mainland China an ideal region for investigating the spatiotemporal evolution and regional differences of heatwaves.

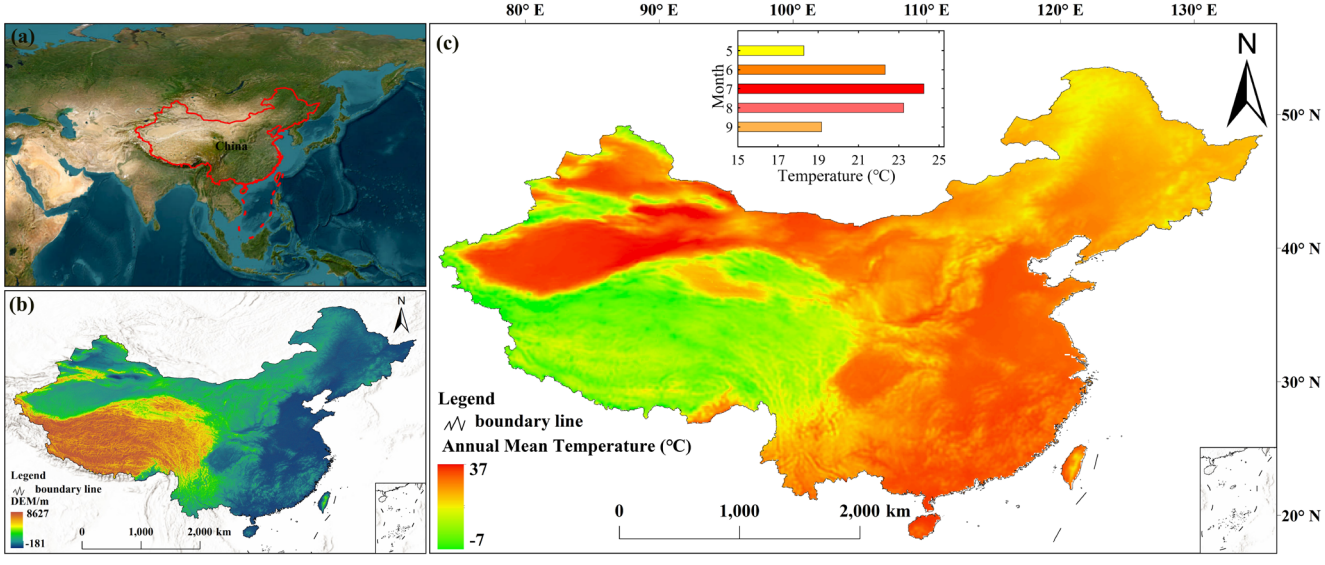

Figure 1. Geographic setting and temperature background of mainland China. (a) Location of the study area; (b) topography; (c) spatial distribution of mean daily maximum temperature during May–September, with the inset bar showing its intra-seasonal variation.

2.2 Datasets

In this study, 2 m air temperature data were obtained from the ERA5-Land reanalysis dataset provided by the European Centre for Medium-Range Weather Forecasts (ECMWF). The dataset has a spatial resolution of 0.1° and an hourly temporal resolution, covers the global land surface, and is well suited for characterizing the spatiotemporal variability of near-surface air temperature (Muñoz-Sabater et al., 2021). Previous studies have shown that ERA5-Land 2 m air temperature data are highly consistent with ground-based observations across most land areas in China and worldwide, and are therefore suitable for the identification of extreme high-temperature events and related research (Muñoz-Sabater et al., 2021; Zhao et al., 2023; Zou et al., 2022; Yilmaz, 2023; Araújo et al., 2022). Hourly 2 m air temperature was aggregated to daily maximum temperature before heatwave identification.

https://doi.org/10.5194/egusphere-2026-3287
Preprint. Discussion started: 24 June 2026

2.3 Method

2.3.1 Identifying heatwave events based on 3D clustering algorithm

To account for the persistence of high-temperature episodes, the operational criterion used in China's heat warning system for consecutive hot days, and the need for seasonally adaptive identification under different regional climatic backgrounds, this study defined a heat event at each grid cell as a period during which the daily maximum temperature exceeded the calendar-day-specific 90th percentile threshold, smoothed using a 15-day moving window, for at least three consecutive days (Awasthi et al., 2022). Given that heatwaves in China occur predominantly from May to September, this study identified heatwave events across mainland China during the May–September period from 1986 to 2024 (Shi et al., 2024a; Wei et al., 2023; Yu et al., 2021). On this basis, an improved three-dimensional clustering algorithm was employed to identify heatwave events within the continuous longitude-latitude-time framework (Guo et al., 2018), thereby preserving their spatiotemporal continuity and characterizing their morphological and dynamic evolution.

First, using daily maximum temperature as the base variable, a three-dimensional temperature data cube of size $N_{lat} \times N_{lon} \times N_t$ was constructed, where N_{lat}, N_{lon}, and N_t represent the numbers of latitudinal grids, longitudinal grids, and the length of the time series (days), respectively (Figure 2a). Subsequently, at each daily time step, grid cells exceeding the corresponding threshold were labelled as hot-temperature pixels, and spatially contiguous daily hot-temperature patches were identified (Gu et al., 2025; Zhang et al., 2025). To emphasize regionally continuous heat processes and reduce interference from locally isolated hot-temperature patches, this study drew on previous research (Guo et al., 2018; Xu et al., 2015; Wang et al., 2011). Only hot-temperature patches with an area exceeding 1.6% of the land area of mainland China (1.52×10^5 km²) were retained. On this basis, the overlapping area between hot-temperature patches on two consecutive days was further calculated. When the overlapping area exceeded 6400 km², the patches were regarded as the continuous evolution of the same heatwave event on adjacent days; otherwise, they were treated as different events(Ren et al., 2025; Guo et al., 2018; Sánchez-Benítez et al., 2020). By repeating the above matching procedure along the temporal dimension, each three-dimensional connected component with a duration of no less than 3 days was assigned a unique identifier, thereby yielding the set of three-dimensional heatwave events for the study period (Tan et al., 2024; Shi et al., 2024b; Dar and Apurv, 2024). The identification procedure for a complete three-dimensional heatwave event is illustrated in Figure 2b.

https://doi.org/10.5194/egusphere-2026-3287
Preprint. Discussion started: 24 June 2026

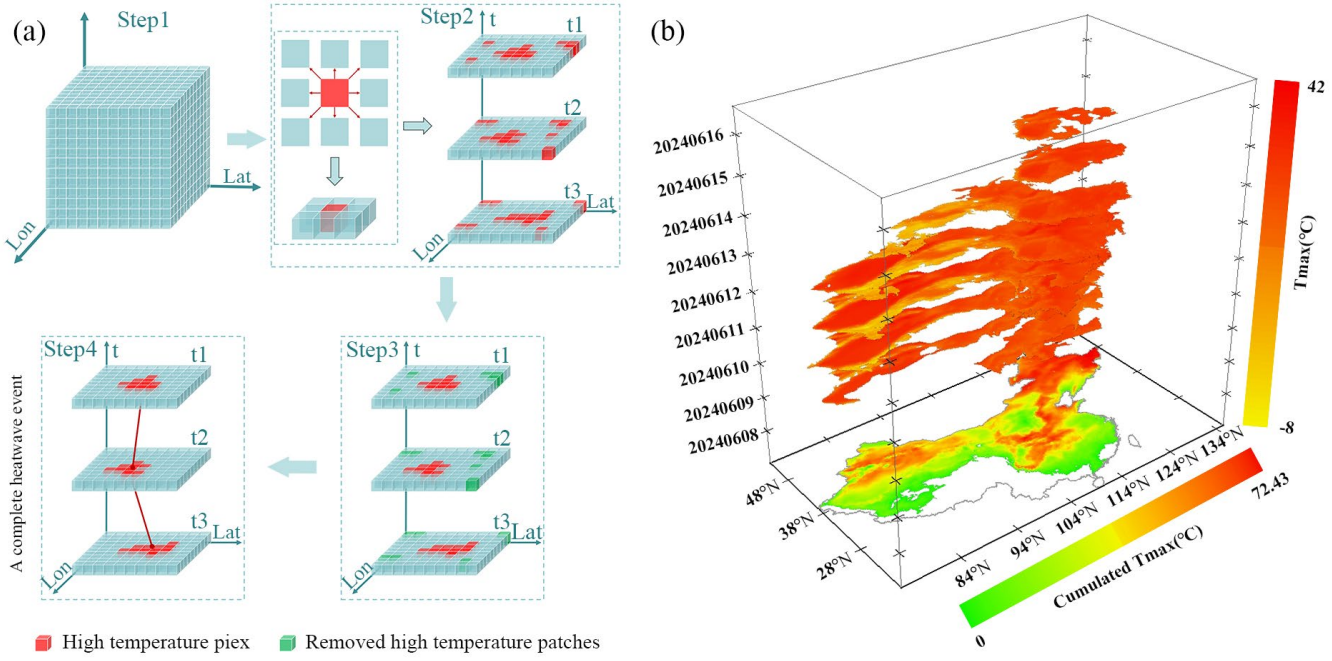

Figure 2. Spatiotemporally contiguous heatwave event identification and 3D structure. (a) Workflow for identifying spatiotemporally contiguous heatwave events using the 3D clustering algorithm; (b) The 3D structure of a typical heatwave event occurred in June 2024.

2.3.2 Heatwave event characteristic indicators

To systematically quantify the spatiotemporal process characteristics of three-dimensional heatwave events, this study developed an indicator system from the perspectives of event occurrence, persistence, severity, spatial extent, and mobility. The indicators include heatwave frequency (HWF), heatwave duration (HWD), heatwave severity (HWS), heatwave area (HWA), heatwave centroid (HWC), heatwave track length (HWL), heatwave intensity (HWI), and heatwave moving speed (Speed), as listed in Table 1.

https://doi.org/10.5194/egusphere-2026-3287
Preprint. Discussion started: 24 June 2026

Table 1. Definitions and units of the key metrics used to characterize 3D heatwave events.

Abbreviation	Full name	Definition	Unit	Equation
HWF	Heatwave frequency	Total number of heatwave events identified.	events	Count of events
HWD	Heatwave duration	Duration of a single heatwave event from onset to termination.	days	$HWD = t_{end} - t_{start} + 1$
HWS	Heatwave severity	Cumulative severity of a single heatwave event over its lifetime.	°C days km^2	$HWS = \sum_{t=1}^{DD}\left(\sum_{i=1}^{N_t}\left(\left(T_{i,t} - T_{i,t}^{th}\right) \times A_i\right)\right)$
HWI	Heatwave intensity	Mean severity of a single heatwave event.	°C km^2	$HWI = \frac{HWS}{HWD}$
HWA	Heatwave area	Event-affected area of a single heatwave event.	km^2	$HWA = \sum_{i=1}^{N_t} A_i$
HWC	Heatwave centroid	Centroid position of the heatwave event at each time step.	longitude, latitude	$Lon_t = \frac{\sum_{i=1}^{N_t} \omega_{i,t} lon_i}{\sum_{i=1}^{N_t} \omega_{i,t}}, Lat_t = \frac{\sum_{i=1}^{N_t} \omega_{i,t} lat_i}{\sum_{i=1}^{N_t} \omega_{i,t}}$
HWL	Heatwave track length	Total travel distance of a single heatwave event over its lifetime.	km	$HWL = \sum_{t=1}^{DD-1} d_t$
Speed	Heatwave moving speed	Mean moving speed of a single heatwave event over its lifetime.	km day^{-1}	$Speed = \frac{HWL}{HWD}$

https://doi.org/10.5194/egusphere-2026-3287
Preprint. Discussion started: 24 June 2026

Where i denotes the affected grid cell, t denotes the time step, N_t is the number of affected grid cells at time step t, A_i is the area of grid cell i, $T_{i,t}$ is the daily maximum temperature of grid cell i at time step t, $T_{i,t}^{th}$ is the corresponding heatwave threshold, DD is event duration, and $\omega_{i,t}$ is the weighting factor used for centroid calculation, d_t denotes the distance between the centroids at times t and $t+1$.

3 Results

3.1 Identification of the rapid-warming stage and phase division across mainland China

From 1986 to 2024, the annual mean daily maximum temperature over mainland China exhibited an overall upward trend, although the warming rate differed markedly among the three phases (Figure 3). From 1986 to 1998, the annual mean daily maximum temperature increased slowly, with a linear trend of 0.03 °C yr^{-1}. During 1999–2011, the warming rate increased slightly, with a slope of 0.04 °C yr^{-1}. In contrast, the warming rate rose further to 0.09 °C yr^{-1} during 2012–2024, approximately 2–3 times higher than that in the previous two phases, indicating that mainland China entered a more pronounced period of rapid warming after 2012. Meanwhile, the fitted trend in the third phase was more stable and the warming signal was clearer, indicating that over the past decade or so, the warming process has become not only stronger in magnitude but also more persistent.

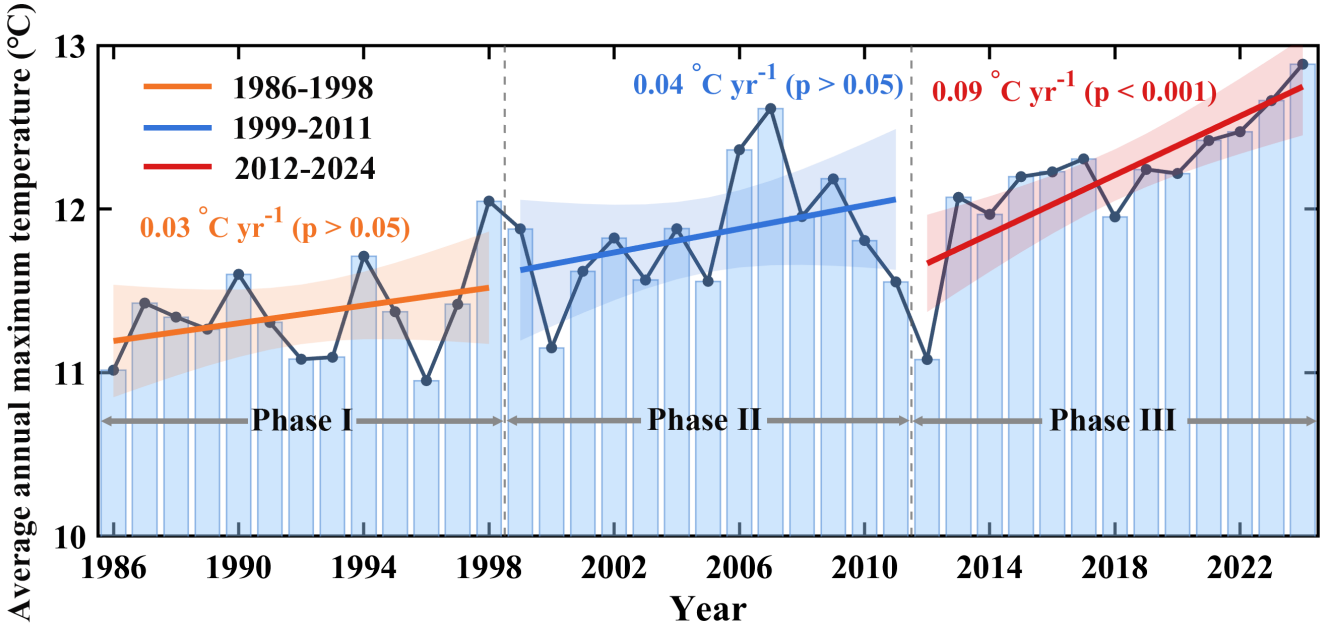

Figure 3. Interannual variation in annual mean daily maximum temperature across mainland China during 1986–2024.

https://doi.org/10.5194/egusphere-2026-3287
Preprint. Discussion started: 24 June 2026

The breakpoint test results further support the above phase division. Both the Pettitt test and the sensitivity analysis indicate that 2012 was a significant turning point in the variation of annual mean daily maximum temperature over mainland China (Figure S1 and Table S1). Spatially, the area experiencing warming during 2012–2024 accounted for 96.7% of mainland China, the highest among the three phases. Of this, the proportion of significantly warming areas reached 39.60%, which was also higher than that in the previous two phases (Figure S2). Li et al. (2019) also found that the rate of global warming slowed during 1998–2012, a period commonly referred to as the "global warming hiatus" or "warming slowdown," which is broadly consistent with the phase-specific variation in annual mean maximum temperature observed in China. Accordingly, the period 1986–2024 was divided into three phases: 1986–1998 (Phase I), 1999–2011 (Phase II), and 2012–2024 (Phase III). This phase division not only accounts for the abrupt change characteristics of the temperature series, but also ensures temporal continuity and inter-phase comparability, thereby providing a reliable basis for subsequent analyses of the spatiotemporal evolution of heatwaves across different phases.

3.2 Joint intensification of multiple characteristics in 3D heatwave events across warming phases

Based on the improved three-dimensional clustering method, a total of 609 three-dimensional heatwave events were identified across mainland China during 1986–2024. Among them, 177, 219, and 213 events were identified in Phase I, Phase II, and Phase III, respectively (Figure 4a). The numbers of events in both Phase II and Phase III were higher than that in Phase I; however, changes in the total number of events alone are insufficient to fully capture the phase-specific evolution of three-dimensional heatwave events.

In terms of duration structure, heatwave events in all three phases were dominated by short-duration events, among which 3–6-day events consistently accounted for the largest proportion, representing 63.8%, 61.1%, and 60.1% in Phase I, Phase II, and Phase III, respectively. The corresponding proportions of 7–10-day events were 27.8%, 23.3%, and 22.5% (Figure 4b). Compared with Phase I, the proportion of short-duration events generally decreased in Phases II and III, whereas the proportion of longer-duration events increased steadily. Specifically, the proportion of 11–20-day events increased from 7.3% in Phase I to 14.2% in Phase II and, although it declined slightly to 12.7% in Phase III, remained markedly higher than that in Phase I. The proportion of 21–30-day events increased from 1.1% to 1.4% and 3.3%, respectively. Events lasting 31–45 days were nearly absent or accounted for only a negligible proportion in Phases I and II, but increased to 1.4% in Phase III. These changes indicate that the proportion of long-duration events increased across the three phases.

In terms of distributional characteristics, the boxplots of HWD further confirm this changing trend (Figure 4c). Although the median HWD changed only modestly across the three phases and remained concentrated within the short-duration range, the upper whisker in Phase III was markedly higher, with more high-value outliers and a greater upper bound of duration. This indicates that long-duration events occurred more frequently in the later period, resulting in a pronounced extension of the upper tail of the HWD distribution. Meanwhile, the boxplots of HWS show that the distributions in Phases II and III were overall higher than that in Phase I, with the high-value tail being most strongly extended in Phase III and the number of

https://doi.org/10.5194/egusphere-2026-3287
Preprint. Discussion started: 24 June 2026

extreme high-value events increasing markedly (Figure 4d). This suggests that three-dimensional heatwave events not only tended to persist longer, but also exhibited a pronounced increase in cumulative severity during the later period.

From a phase-comparison perspective, the evolution of heatwave events was reflected primarily in the increasing proportion of long-duration events and the intensification of event severity, rather than in a continued rise in the total number of events. Particularly in Phase III, although the total number of events decreased slightly relative to Phase II, the contributions of long-duration and high-severity events increased further, indicating that the evolution of three-dimensional heatwave processes over mainland China has gradually shifted from a pattern dominated by increasing event counts to one characterized by longer persistence and stronger impacts.

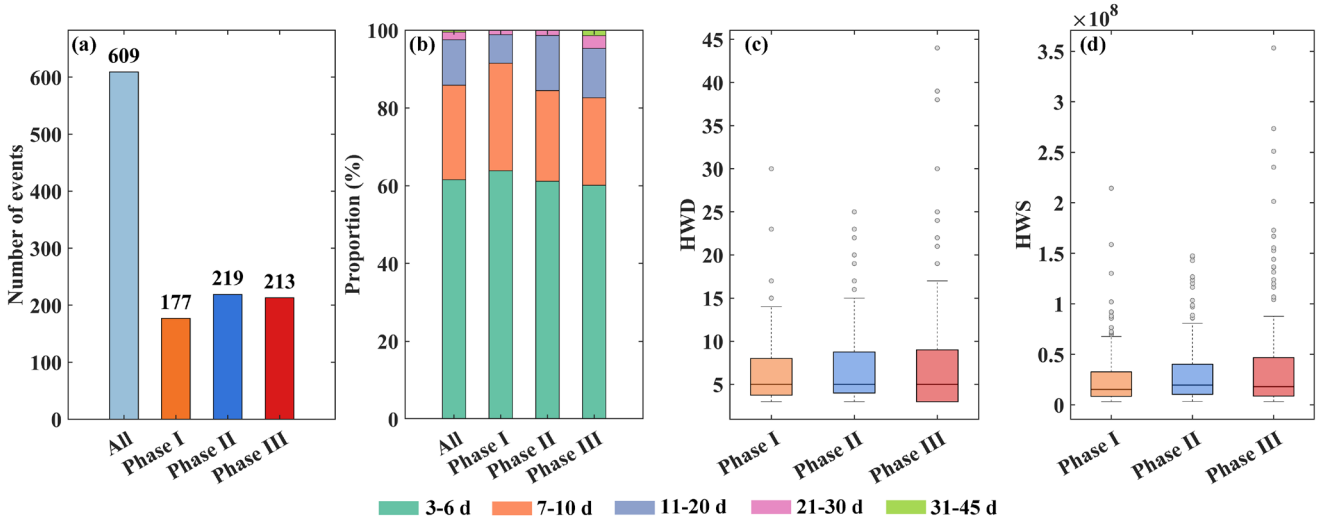

Figure 4. Phase-wise changes in duration classes and severity distributions of 3D heatwave events across mainland China during 1986–2024. (a) Number composition of heatwave events across duration classes for all events and each phase. (b) Proportional composition of heatwave events across duration classes for all events and each phase. (c) Distribution of heatwave duration (HWD) across the three phases. (d) Distribution of heatwave severity (HWS) across the three phases.

This increasing proportion of long-duration events was accompanied by the concurrent intensification of multiple key heatwave characteristics. As shown in Figure 5, the fitted slopes of HWF, HWD, HWS, HWA, HWL, and Speed were positive across the three phases, indicating that heatwaves over mainland China exhibited overall increasing trends in frequency, duration, severity, affected area, track length, and moving speed during 1986–2024. However, the magnitude of increase differed among the indicators. Compared with Phases I and II, Phase III exhibited more pronounced increases in multiple characteristics, with the most notable amplification observed in HWD, HWS, HWA, and HWL. Specifically, the rate of change in HWD increased markedly from 0.074 days yr^{-1} in Phase I and 0.046 days yr^{-1} in Phase II to 0.264 days yr^{-1} in Phase III. HWL increased from 49.575 km yr^{-1} and 8.234 km yr^{-1} to 116.060 km yr^{-1}, HWA from 5×10^4 km^2 yr^{-1} and 6×10^4 km^2 yr^{-1} to 1×10^5 km^2 yr^{-1}, and HWS from 9×10^5 °C days km^2 yr^{-1} and 4×10^5 °C days km^2 yr^{-1} to 2.6×10^6 °C days km^2 yr^{-1}. By contrast, although HWF also exhibited an increasing trend, its rate of increase was relatively limited, suggesting

https://doi.org/10.5194/egusphere-2026-3287
Preprint. Discussion started: 24 June 2026

that the recent intensification of heatwaves was driven less by a continued rise in event counts than by the strengthening of event-level characteristics.

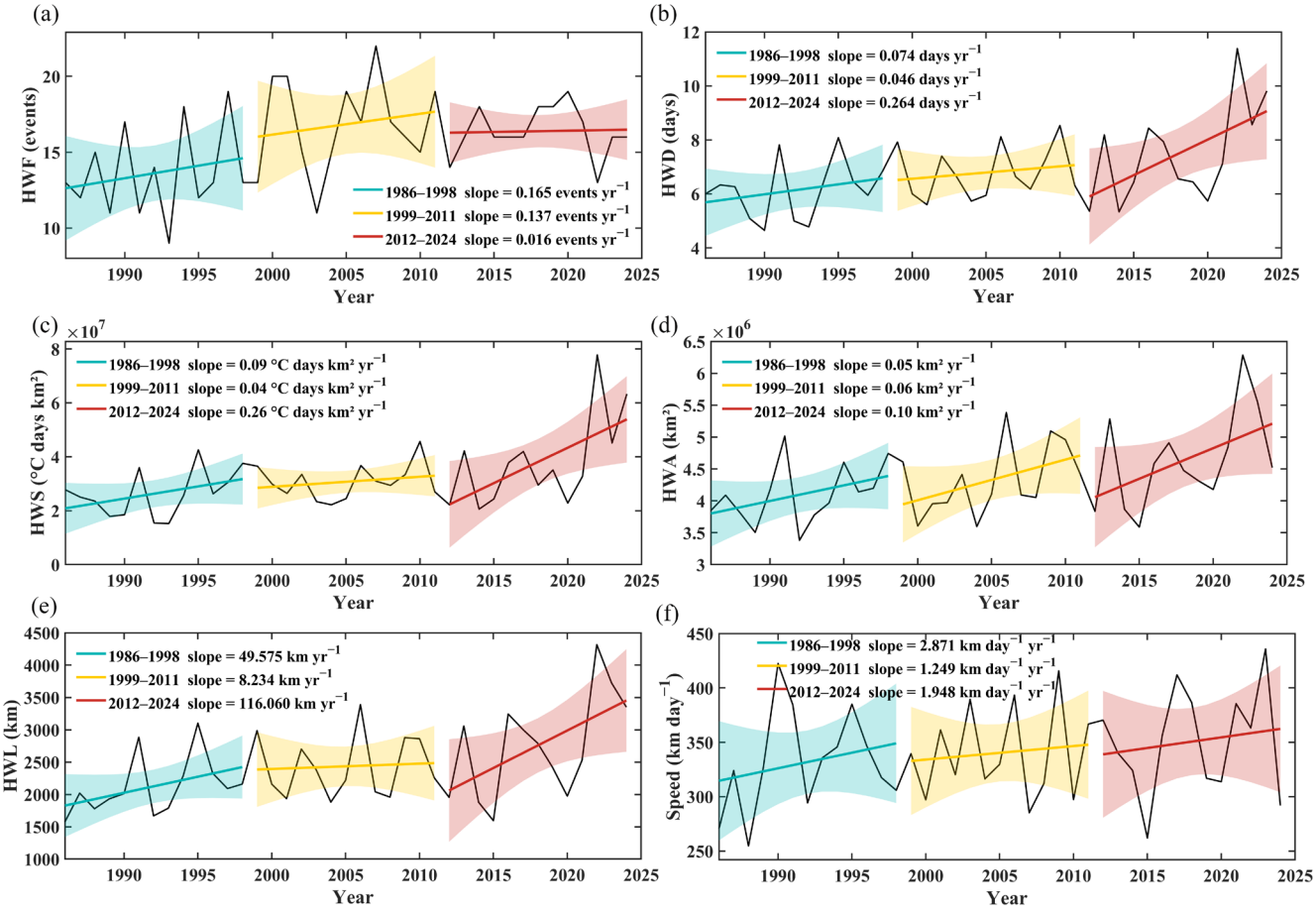

Figure 5. Phase-wise changes in six key heatwave characteristics across mainland China during 1986–2024.

https://doi.org/10.5194/egusphere-2026-3287
Preprint. Discussion started: 24 June 2026

Table 2. Summary statistics of 3D heatwave events and changes in key characteristics across the three phases (* represents $p < 0.1$).

	Proportion of different time periods		Slope of HWF (events yr^{-1})	Slope of HWD (days yr^{-1})	Slope of HWS (10^7 °C days km^2 yr^{-1})	Slope of HWA (10^6 km^2 yr^{-1})	Slope of HWL (km yr^{-1})	Slope of Speed (km day^{-1} yr^{-1})
Phase I	3–6 d	63.8%	0.165	0.074	0.09	0.05	49.575	2.871
	7–10 d	27.8%						
	11–20 d	7.3%						
	21–30 d	1.1%						
	31–45 d	0						
Phase II	3–6 d	61.1%	0.137	0.046	0.04	0.06	8.234	1.249
	7–10 d	23.3%						
	11–20 d	14.2%						
	21–30 d	1.4%						
	31–45 d	0						
Phase III	3–6 d	60.1%	0.016	0.264*	0.26*	0.10*	116.06*	1.948
	7–10 d	22.5%						
	11–20 d	12.7%						
	21–30 d	3.3%						
	31–45 d	1.4%						

https://doi.org/10.5194/egusphere-2026-3287
Preprint. Discussion started: 24 June 2026

Compared with the previous two phases, Phase III exhibited greater increases in HWD, HWS, HWA, and HWL. During this phase, heatwave events were characterized not only by longer duration, greater cumulative severity, and broader affected areas, but also by a marked increase in track length (Figure 5; Table 2). These results indicate that changes in heatwaves during the rapid warming phase involved multiple characteristics, including duration, severity, affected area, and track length.

3.3 Relationships of heatwave migration with duration, severity, and affected area

Figure 6 shows the distribution of migration directions of heatwave events over mainland China during 1986–2024 and across the three phases, as well as the differences in duration composition among different migration directions. Overall, during 1986–2024, the migration directions of heatwave events were dominated by eastward (E) and southeastward (SE) movement, accounting for 30.6% and 24.5% of all events, respectively. Together, these two directions represented more than 50% of the total, indicating that heatwave events over mainland China were characterized primarily by eastward and southeastward migration (Figure 6a, b). From a phase-based perspective, the migration directions exhibited clear inter-phase differences. In Phase I, the directional distribution was relatively concentrated, with eastward (E) and southeastward (SE) movements accounting for 33.0% and 30.7% of all events, respectively, for a combined proportion of 63.7%. In Phase II, the directional distribution became more dispersed, with the proportions of events moving in directions other than E and SE increasing to varying degrees. Upon entering Phase III, the migration directions became more concentrated again, with the proportions of events moving in the E, SE, northwestward (NW), and northward (N) directions all showing an increase (Figure 6e, h, k). The duration composition across different migration directions further indicates that E and SE were not only the most common directions of heatwave movement, but also major directions associated with longer-duration events. As the phases progressed, event duration increased continuously in the E, N, and NW directions, and by Phase III, extremely long-duration events had begun to emerge in the E, southwestward (SW), and SE directions (Figure 6c, f, i, l).

https://doi.org/10.5194/egusphere-2026-3287
Preprint. Discussion started: 24 June 2026

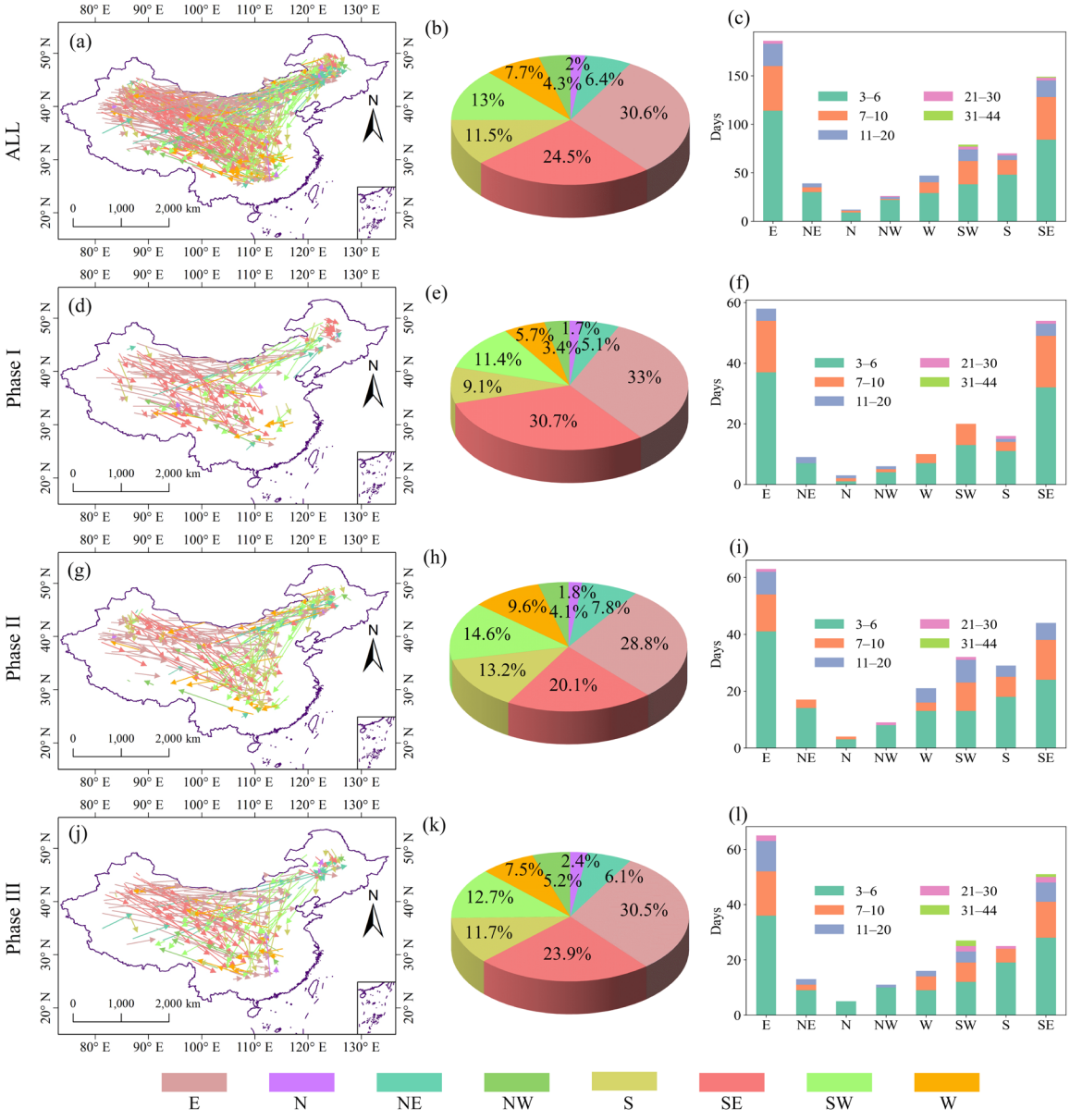

Figure 6. Movement directions and duration classes of heatwave events across mainland China during different warming phases.

Compared with the distribution of migration directions, the relationship between track length and other event characteristics more directly reflects the role of mobility in heatwave intensification. Figure 7 shows that during 1986–2024, HWL was significantly positively correlated with HWS, HWD, and HWA ($p < 0.01$), with correlation coefficients of 0.81, 0.87, and 0.78, respectively. Among these relationships, the strongest correlation was observed between HWL and HWD (Figure 7a–c). As HWL increased, both HWS and HWA showed an overall upward trend, indicating that long-track events tended to be associated with greater cumulative severity and broader affected areas. The fitted results show that all three relationships

https://doi.org/10.5194/egusphere-2026-3287
Preprint. Discussion started: 24 June 2026

were nonlinear. When HWL exceeded approximately 1×10^4 km, the rates of increase in both HWD and HWS became even steeper.

A phase-based comparison further indicates that the above relationships exhibited a pattern of continued strengthening over time. In Phase I, the correlation coefficients between HWL and HWS, HWD, and HWA were 0.78, 0.80, and 0.77, respectively. In Phase II, the corresponding values were 0.77, 0.84, and 0.78, and in Phase III they further increased to 0.84, 0.90, and 0.80. Notably, the correlation between HWL and HWD reached its highest value among the three phases in Phase III (Figure 7d–l). A phase-based comparison shows that the correlations of HWL with HWD, HWS, and HWA were stronger in Phase III.

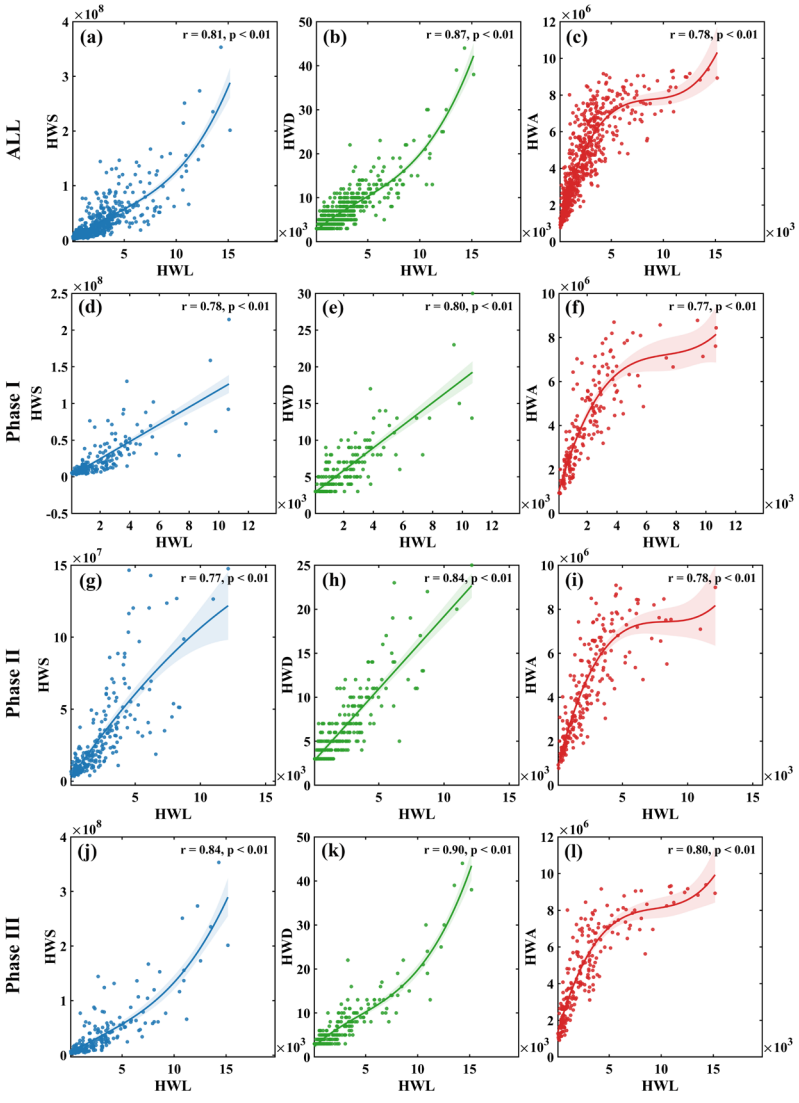

Figure 7. Relationships between heatwave track length (HWL) and duration (HWD), severity (HWS), and affected area (HWA) during different warming phases.

https://doi.org/10.5194/egusphere-2026-3287
Preprint. Discussion started: 24 June 2026

By contrast, the relationships between Speed and HWS, HWD, and HWA were generally weaker (Figure S6). During 1986–2024, the correlation coefficients of Speed with HWS, HWD, and HWA were 0.25, 0.21, and 0.60, respectively, and the fitted relationships generally exhibited a nonlinear inverted U-shaped pattern. As the phases progressed, the correlation between Speed and HWA increased to some extent, whereas its relationships with HWS and HWD remained consistently weak. Overall, track length was more closely associated with heatwave duration, cumulative severity, and spatial extent, whereas moving speed primarily reflected the spatial expansion of events and played a relatively limited role in heat accumulation and persistence.

3.4 Spatial expansion of heatwave intensification and intra-seasonal phase differences

From the perspective of spatial distribution, the intensification of heatwaves over mainland China was manifested not only in the increasing duration, severity, and track length of events at the event scale, but also in the continuous expansion of the spatial extent affected by heatwaves. According to Figures S4 and S5, both the annual mean heatwave days and cumulative heatwave temperature over mainland China exhibited clear phase-dependent intensification during 1986–2024. Overall, except for the Tibet Autonomous Region and parts of northeastern China, most regions of mainland China showed increases in annual mean heatwave days and cumulative heatwave temperature, with the spatial extent of high-value areas continuing to expand. During Phase I, the annual mean cumulative heatwave temperature across most regions of China was primarily distributed within 0–60 °C yr^{-1}, while the annual mean number of heatwave days was mainly concentrated within 10–30 days yr^{-1}. Upon entering Phase II, the annual mean cumulative heatwave temperature across most regions of China increased to 60–120 °C yr^{-1}, while the annual mean number of heatwave days rose to 20–40 days yr^{-1}. In addition, the spatial extent of high-value areas expanded further relative to that in Phase I. In Phase III, heatwaves intensified further and exhibited a more pronounced southward expansion. Across most regions of China, the annual mean cumulative heatwave temperature remained mainly within 60–120 °C yr^{-1}, but its spatial coverage expanded further. At the same time, the annual mean number of heatwave days increased to 30–50 days yr^{-1}, and the area of high-value regions also increased significantly (Figures S4 and S5). These results indicate that, during the phase-wise evolution, heatwaves over mainland China were characterized by persistent intensification, an expanding affected area, and a southward shift of high-value regions.

The spatial distribution of inter-phase differences further indicates that this intensification exhibited strong regional consistency. As shown in Figure 8, relative to Phase I, both heatwave days and cumulative heatwave temperature exhibited positive increases across most regions of mainland China in Phase II, except for parts of the Tibet Autonomous Region. Compared with Phase II, both indicators increased further across most regions of mainland China in Phase III, except for parts of northeastern China. Compared with Phase I, nearly the entire region of mainland China experienced marked increases in both heatwave days and cumulative heatwave temperature in Phase III (Figure 8). These difference patterns indicate that the spatial extent of heatwave intensification expanded progressively across the successive phases.

https://doi.org/10.5194/egusphere-2026-3287
Preprint. Discussion started: 24 June 2026

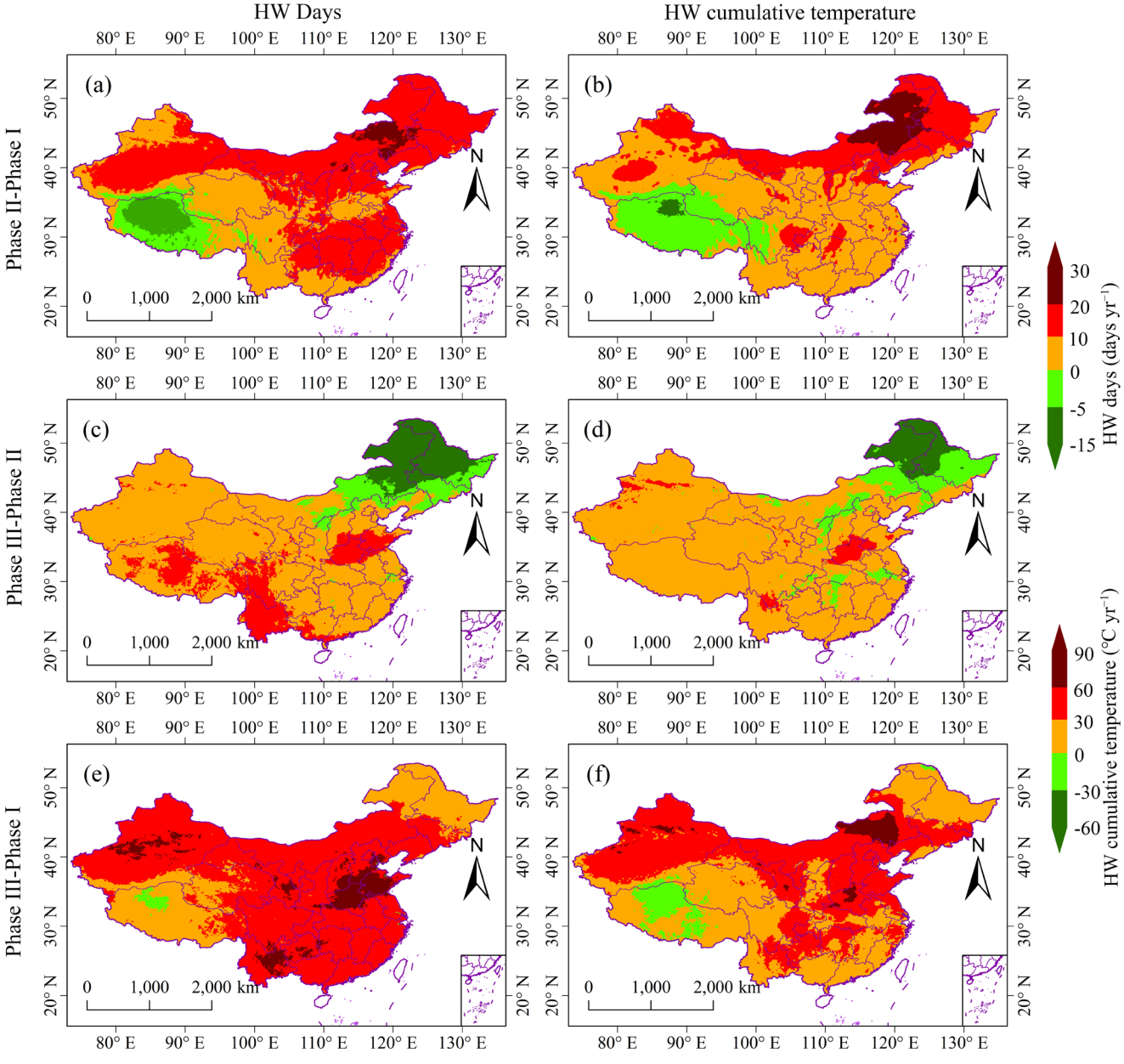

Figure 8. Inter-phase differences in annual heatwave days and cumulative heatwave temperature across mainland China.

In addition to the spatial expansion, heatwave characteristics from May to September also exhibited pronounced month-to-month variability within the warm season. As shown in Figure 9, the six heatwave characteristic indicators during 1986–2024 were not consistent across different months. In May, heatwaves exhibited the highest severity (HWS = 4.2×10^7 °C days km^2) and the largest affected area (HWA = 5.1×10^6 km^2). At the same time, both track length and movement speed reached their maximum values, indicating that although heatwaves in May were not the most frequent, they tended to be more

https://doi.org/10.5194/egusphere-2026-3287
Preprint. Discussion started: 24 June 2026

intense, spatially more extensive, and faster moving. In June, heatwaves were characterized by the highest frequency (HWF=136 events) but the shortest duration (HWD=6.4 days), indicating that heatwave activity in this month was more strongly characterized by frequent but short-lived events. In July, heatwaves had the longest duration (HWD = 7.2 days), whereas both severity and affected area declined to some extent, indicating that heatwave activity during this period was characterized more by enhanced persistence than by a simultaneous increase in extreme intensity. In August, HWS, HWF, HWA, and Speed were generally at relatively low levels, whereas all heatwave characteristics showed a certain degree of rebound in September (Figure 9). Overall, heatwaves over mainland China during the warm season did not follow a single, uniform seasonal evolution pattern; instead, they exhibited clear month-to-month differences, characterized by stronger events in May, more frequent events in June, longer-lasting events in July, weaker activity in August, and a rebound in September.

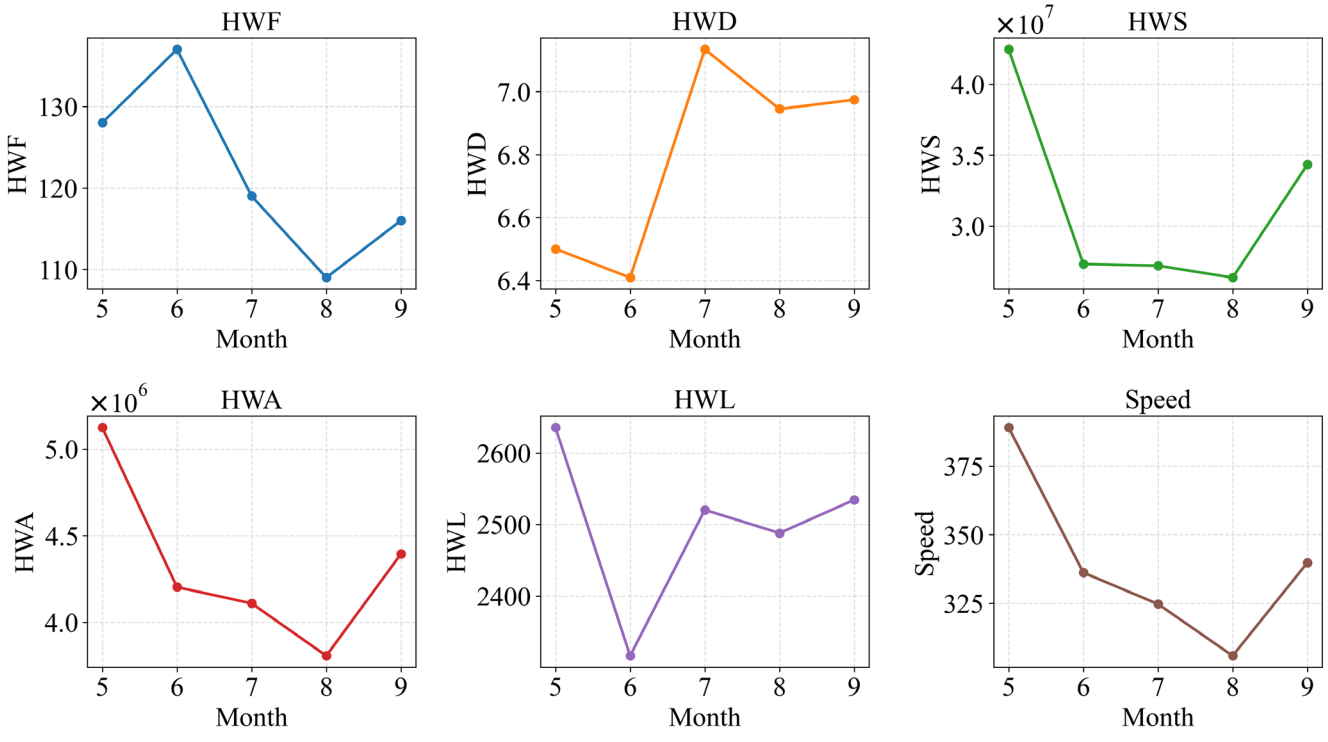

Figure 9. Monthly variation in key heatwave event characteristics during May–September of 1986–2024.

Further phase-based comparisons indicate that the month-to-month variability within the warm season also exhibited a pronounced pattern of intensification across phases. Figure S12 shows that although the magnitude of intensification differed among months, Phase III generally exhibited greater increases in heatwave characteristics in most months. Specifically, in May, the slopes of HWD, HWS, and HWL in Phase III were all higher than those in Phases I and II. In June, Phase III exhibited the most comprehensive intensification, with the slopes of HWF, HWD, HWS, HWA, and HWL all exceeding those in the previous two phases. Phase III in July likewise exhibited pronounced intensification, with HWD, HWS, HWA,

https://doi.org/10.5194/egusphere-2026-3287
Preprint. Discussion started: 24 June 2026

HWL, and Speed all showing marked increases relative to the previous two phases. Although the overall magnitude of intensification was relatively weaker in August, the slopes of HWS and Speed still reached higher values in Phase III. In September, the most prominent increases were observed in HWD, HWS, and HWL. Although Phase III generally exhibited greater increases in most months, the primary indicators of change were not identical across months.

Overall, during the phase-wise evolution, heatwaves over mainland China were characterized not only by the continuous expansion of their affected area, but also by pronounced month-to-month variability within the warm season and a clear phase-dependent intensification of these intra-seasonal differences. The spatial expansion indicates that heatwave intensification has progressed from localized high-value regions to broader areas, whereas the month-to-month differences suggest that this intensification has not occurred uniformly within the warm season, but instead exhibits a pronounced intra-seasonal structure (Figures 8 and 9; Figures S4, S5, and S12).

3.5 Phase comparison of representative three-dimensional heatwave events

To more intuitively illustrate the differences in persistence, spatial expansion, and migration trajectory of three-dimensional heatwave events across different warming phases, this study selected the most severe representative event in each of Phase I, Phase II, and Phase III, as measured by HWS, for comparative analysis (Figure 10; Figures S13 and S14). All three events exhibited pronounced spatial migration and changes in affected extent, but differed markedly in duration, cumulative severity, and spatial coverage, thereby providing process-based visual evidence for the phase-dependent intensification identified in the preceding statistical analysis.

The representative event in Phase I occurred from 5 May to 3 June 1995 and lasted for 30 days (Figure 10a). At the initial stage of the event, heatwave activity was concentrated mainly in northeastern and northwestern China. It then gradually expanded southward and underwent spatial migration, resulting in the development of high cumulative-temperature centres over southwestern China and parts of central China, with a maximum cumulative temperature of 149 °C. In terms of its trajectory, the event originated near the border between Gansu Province and the Inner Mongolia Autonomous Region and eventually dissipated in southern Qinghai Province. Its centroid activity was concentrated mainly in western China, particularly in the Qinghai-Tibet region (Figure 10b). During the event, the temporal variations in HWS, HWA, and HWI were generally highly consistent, although the peak timings of the different indicators were not fully synchronized. Specifically, the maxima of HWS, HWA, and HWI occurred on 7 May, 31 May, and 19 May 1995, respectively (Figure 10c).

https://doi.org/10.5194/egusphere-2026-3287
Preprint. Discussion started: 24 June 2026

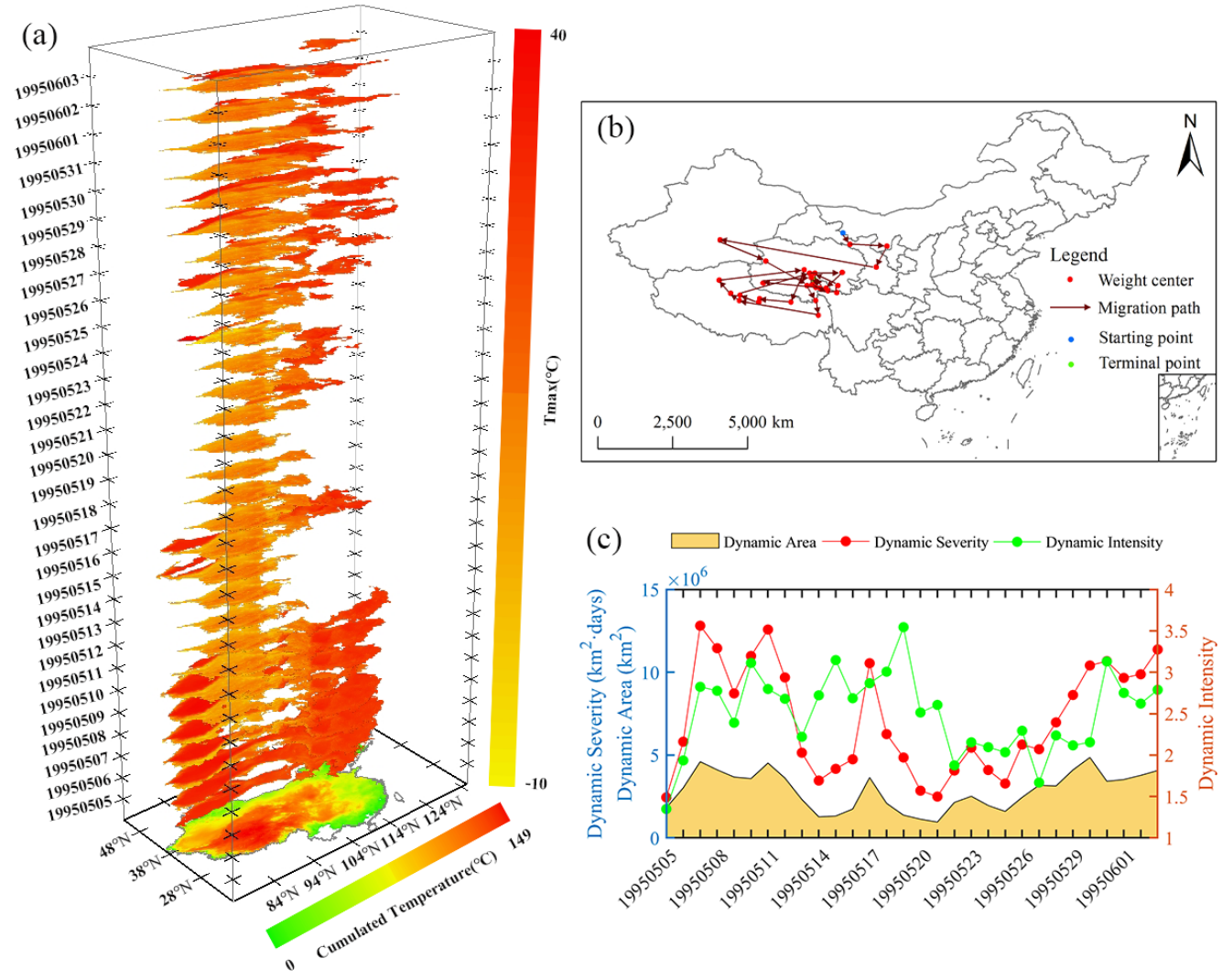

Figure 10. Representative 3D heatwave event with the highest HWS during Phase I (5 May–3 June 1995).

The representative event in Phase II occurred in 2010 and lasted for 25 days, giving it a shorter overall duration than the Phase I event (Figure S13). This event originated in southwestern Inner Mongolia and eventually dissipated in southeastern Chongqing, with its centroid activity concentrated mainly in central and northeastern China (Figures S13a and S13b). In terms of spatial evolution, the event was likewise concentrated mainly in northwestern and northeastern China during its initial stage and then gradually expanded southward. However, the high-value centres of cumulative temperature remained located primarily in northeastern China, with a maximum cumulative temperature of 81 °C, which was substantially lower than that of the representative events in Phases I and III. Correspondingly, HWS, HWA, and HWI generally exhibited a temporal pattern of initial intensification followed by weakening, with their peak values occurring on 25 June, 27 June, and 5 July 2010, respectively (Figure S13c). Compared with Phase I, the representative event in this phase did not exhibit a further

https://doi.org/10.5194/egusphere-2026-3287
Preprint. Discussion started: 24 June 2026

increase in duration or cumulative impact; rather, it was characterized by more concentrated temporal fluctuations and a shorter period of peak intensity.

The representative event in Phase III occurred from 14 August to 26 September 2024 and lasted for 44 days, markedly longer than the representative events in the previous two phases, making it the longest-lasting of the three events (Figure S14a). This event originated in Xinjiang and then continued to expand eastward, exhibiting pronounced stalling over Qinghai, Sichuan, Shanxi, Hunan, and Ningxia, before eventually dissipating within Qinghai Province (Figure S14b). Compared with the representative events in the previous two phases, this event exhibited larger fluctuations in HWS and HWA and markedly higher overall levels. Its high-value centres of cumulative temperature were located mainly in northwestern China as well as parts of central and eastern China, with a maximum cumulative temperature of 149 °C. This value was substantially higher than that of the Phase II event and comparable to the peak level in Phase I, but was accompanied by a longer duration and greater process intensity (Figure S14c). This event indicates that in Phase III, long duration, high severity, and broad spatial extent could occur simultaneously within a single heatwave process, consistent with the concurrent intensification of multiple heatwave characteristics revealed by the preceding statistical analysis.

Overall, the representative events in all three phases exhibited pronounced spatial migration and changes in affected extent, whereas the Phase III event was characterized by a longer duration and greater process variability. Compared with Phases I and II, Phase III was associated not only with longer event duration, but also with a greater tendency to produce continuous heatwave processes characterized by sustained spatial expansion and higher cumulative severity (Figure 10; Figures S13 and S14). Therefore, the comparison of representative events further corroborates, from a process-based perspective, the conclusion drawn from the overall statistical analysis: after 2012, the intensification of heatwaves over mainland China was manifested more in the concurrent enhancement of multiple event characteristics, including persistence, severity, and spatial extent, rather than in a localized increase in any single indicator.

4 Discussion

4.1 Coordinated intensification of event characteristics in contiguous heatwaves under rapid warming

Previous studies have generally indicated that under persistent warming, heatwaves show overall increasing trends in frequency, duration, and intensity (Marengo et al., 2025; Perkins-Kirkpatrick and Lewis, 2020; Wang et al., 2024b). However, these conclusions have been derived largely from statistical analyses at the station or grid-cell scale and have placed greater emphasis on changes in individual indicators. By contrast, this study focuses more on the process-based characteristics of continuous heatwave events themselves. The results indicate that the most prominent change in heatwaves over mainland China after 2012 was not primarily reflected in a continued increase in the number of events, but rather in the concurrent intensification of duration, cumulative severity, affected extent, and track length within the same phase. In other words, changes in heatwaves during the rapid warming phase were no longer manifested merely as an intensification of

https://doi.org/10.5194/egusphere-2026-3287
Preprint. Discussion started: 24 June 2026

localized temperature anomalies, but more importantly as an overall strengthening of continuous processes at the regional scale.

This finding helps to provide a renewed understanding of how heatwaves intensify under a warming climate. If changes in heatwaves are manifested merely as rising local temperatures or increasing event frequency, their impacts are more likely to be reflected in the accumulation of localized or short-term heat exposure. By contrast, when duration, affected extent, and track length increase simultaneously, the characteristics of the corresponding continuous heatwave processes also change accordingly. A longer duration implies that heat stress is sustained for a longer period, a broader affected extent means that more regions are involved in the same process, and a greater track length indicates that the core of the event can continue to migrate over a larger spatial scale (Luo et al., 2022c; Skinner et al., 2025; Sun et al., 2020). This shift from the intensification of isolated temperature anomalies to the concurrent enhancement of multiple event characteristics is consistent with recent findings that heatwaves are becoming longer-lasting, more spatially extensive, and increasingly associated with regional compound exposure (Luo et al., 2024; Skinner et al., 2025). Therefore, the most noteworthy feature of Phase III is not that heatwaves simply became more frequent, but that they increasingly manifested as continuous processes with longer duration, broader spatial extent, and stronger cumulative effects. The results of this study further indicate that these changes did not occur as independent increases in separate characteristics, but emerged in a concentrated manner during the rapid warming phase, suggesting that the intensification of continuous heatwave events over mainland China has shifted from changes in individual characteristics to the concurrent strengthening of multiple event characteristics.

4.2 Migration is a key event characteristic of contiguous heatwave events

With the development of the three-dimensional continuous-event perspective, an increasing number of studies have begun to recognize that heatwaves do not evolve only at fixed local locations, but may instead exhibit pronounced spatial migration, trajectory extension, and regional expansion processes (Gu et al., 2025; Luo et al., 2022a; Luo et al., 2022b; Luo et al., 2022c). However, existing studies have placed greater emphasis on the migration phenomenon itself, while the relationships between heatwave mobility and event persistence, severity, and affected extent have yet to be systematically discussed. The results of this study show that HWL was significantly positively correlated with HWD, HWS, and HWA, with the strongest relationships observed in Phase III; among them, the correlation between HWL and HWD was the highest (Figure 7). Moreover, when HWL exceeded approximately 1×10^4 km, the increases in HWD and HWS became even more pronounced (Figure 7). This suggests that track length is not merely a measure of the spatial displacement of heatwave events, but is also stably associated with their duration, cumulative severity, and affected extent. In other words, heatwaves with longer track length tend to be associated with longer duration, greater cumulative severity, and broader spatial coverage. This result indicates that, in the analysis of continuous heatwave events, track length carries greater process-based significance than moving speed. Traditional studies have often treated duration, intensity, and affected extent as relatively independent outcome indicators. By contrast, the results of this study suggest that, at the scale of continuous heatwave events, these characteristics are not isolated from one another, and that track length may serve as an important process-based indicator

https://doi.org/10.5194/egusphere-2026-3287
Preprint. Discussion started: 24 June 2026

linking them. Particularly in Phase III, the relationships between track length and event duration, severity, and affected extent became even stronger, with long-distance migrating events more likely to correspond to continuous heatwave processes characterized by longer duration, broader spatial extent, and stronger cumulative effects. This understanding is broadly consistent with previous findings that transregional migrating heatwaves are more likely to develop into persistent regional-scale processes (Luo et al., 2024; Wang et al., 2025), and further suggests that mobility should be incorporated into the core indicator system for analysing continuous heatwave processes. It should be noted that this study reveals stable statistical relationships among event characteristics, but does not directly examine the persistence of large-scale atmospheric circulation, land-surface heat maintenance, or land-atmosphere feedback processes that may underpin these relationships (Horowitz et al., 2022).

This study focuses on the statistical and process-based characteristics of contiguous heatwave events. Although the observed strengthening of long-duration and long-track events is likely related to persistent circulation anomalies and land-surface heat maintenance, these mechanisms were not directly diagnosed here. Future work should link the 3D event framework with circulation persistence, soil moisture anomalies, and land-atmosphere feedbacks to clarify the physical drivers of phase-dependent event intensification.

5 Conclusions

By identifying heatwaves over mainland China during May–September of 1986–2024 as contiguous three-dimensional events, this study examined how their key characteristics changed across three warming phases. The results show that recent heatwave change was reflected less in a continued increase in event number than in a phase-dependent strengthening of event processes, particularly after 2012. The main conclusions are as follows:

(1) A total of 609 contiguous heatwave events were identified during 1986–2024, with 177, 219, and 213 events in Phase I (1986–1998), Phase II (1999–2011), and Phase III (2012–2024), respectively. Although the total number of events in Phase III was slightly lower than that in Phase II, the event-duration composition shifted toward longer-lasting events. In particular, the proportion of events lasting 21–30 days increased from 1.4% in Phase II to 3.3% in Phase III, and events lasting 31–45 days increased from 0 to 1.4%, indicating that recent heatwave change was expressed more through the increasing prominence of long-lasting events than through a rise in event counts.

(2) Phase III showed the clearest joint intensification of multiple heatwave characteristics. Compared with the previous two phases, heatwave duration, cumulative severity, affected area, and track length all increased more markedly, whereas the increase in event frequency was relatively limited. This indicates that heatwave intensification over mainland China after 2012 was characterized mainly by longer persistence, stronger cumulative heat stress, broader spatial extent, and greater track length.

(3) Track length carried clearer process-level information than movement speed. During 1986–2024, it was significantly positively correlated with cumulative severity, duration, and affected area ($r = 0.81$, 0.87, and 0.78; $p < 0.01$), and these

https://doi.org/10.5194/egusphere-2026-3287
Preprint. Discussion started: 24 June 2026

relationships were strongest in Phase III (r = 0.84, 0.90, and 0.80). By contrast, movement speed showed much weaker correlations with cumulative severity and duration (r = 0.25 and 0.21), indicating that track length better captures the integrated evolution of contiguous heatwave events.

(4) Heatwave intensification did not occur uniformly within the warm season. Heatwaves in May tended to be stronger and more spatially extensive, those in June were more frequent, and those in July were longer-lasting, whereas activity in August was relatively weaker and intensified again in September. Phase III showed larger increases in most months, indicating that recent heatwave change over mainland China was characterized not only by clear phase dependence, but also by pronounced intra-seasonal differences.

Overall, under rapid warming, heatwaves over mainland China increasingly developed as long-lasting, spatially extensive, and mobile regional processes rather than simply becoming more numerous. This finding highlights the value of examining heatwaves from a contiguous event perspective. At the same time, the physical mechanisms underlying these phase-dependent changes, including the roles of atmospheric circulation persistence and land-atmosphere feedbacks, still require further investigation.

Code and data availability

ERA5-Land 2 m air temperature data are available from the Copernicus Climate Data Store (https://cds.climate.copernicus.eu). The processed heatwave event catalogue, gridded heatwave-day and cumulative-temperature products, plot data supporting all figures and tables, and the scripts used for event identification and analysis have been archived in Zenodo: https://zenodo.org/records/20201003?preview=1&token=eyJhbGciOiJIUzUxMiJ9.eyJpZCI6ImVhMGY3YThmLTU2MzAtNDkwMi05ZjM1LTdiNGRiNDRjZjYzNSIsImRhdGEiOnt9LCJyYW5kb20iOiJlOWU3OGNlNmJhMzRkODZjMGM5ZjA2MTM4M2Q4NjVlNCJ9.l3v-SVgqsmokJVBj9haGk2-PLYUl2v_mJTUxF_PytAfXwicU3MD_urqiGcI1fzTGwh2Kcj9YMHOCSubMDNr80Q. During peer review, access is restricted to reviewers through the repository review link; the archive will be made public upon publication.

Supplement link

Supporting information includes supplementary figures and tables describing breakpoint tests, spatial trends, speed-related relationships, and representative heatwave events in Phases II and III.

Author contributions

Hao Guo: Writing (original draft preparation), Writing (review and editing), Supervision, Software, Methodology, Funding acquisition. Qinghou Hang: Writing (original draft preparation), Visualization, Formal analysis, Data curation,

https://doi.org/10.5194/egusphere-2026-3287
Preprint. Discussion started: 24 June 2026

Conceptualization. Xiangchen Meng: Methodology, Supervision, Resources. Ye Yuan: Resources, Software. Ying Cao: Data curation, Formal analysis, Visualization. Yunqian Wang: Resources, Software, Supervision. Philippe De Maeyer: Conceptualization, Writing (review and editing), Resources, Supervision.

Competing interests

The authors declare that they have no conflict of interest.

Acknowledgements

The authors acknowledge the European Centre for Medium-Range Weather Forecasts (ECMWF) and the Copernicus Climate Data Store (CDS) for providing the ERA5-Land 2m temperature dataset used in this study. The authors gratefully acknowledge the financial support provided by the Natural Science Foundation of Shandong Province, the Rizhao Natural Science Foundation, and the Youth Innovation Teams in Colleges and Universities of Shandong Province.

Financial support

This work was supported by the Natural Science Foundation of Shandong Province (Grant No. ZR2025MS536), the Rizhao Natural Science Foundation (Grant No. RZ2024ZR12), and the Youth Innovation Teams in Colleges and Universities of Shandong Province (2022KJ178).

References

Al-Yaari, A., Zhao, Y., Cheruy, F., and Thiery, W.: Heatwave characteristics in the recent climate and at different global warming levels: A multimodel analysis at the global scale, Earth's Future, 11, e2022EF003301,https://doi.org/10.1029/2022EF003301, 2023.

Araújo, C. S. P. d., Silva, I. A. C. e., Ippolito, M., and Almeida, C. D. G. C. d.: Evaluation of air temperature estimated by ERA5-Land reanalysis using surface data in Pernambuco, Brazil, Environmental Monitoring and Assessment, 194, 381,https://doi.org/10.1007/s10661-022-10047-2, 2022.

Awasthi, A., Vishwakarma, K., and Pattnayak, K. C.: Retrospection of heatwave and heat index, Theoretical and Applied Climatology, 147, 589–604,https://doi.org/10.1007/s00704-021-03854-z, 2022.

Bell, M. L., Gasparrini, A., and Benjamin, G. C.: Climate change, extreme heat, and health, New England Journal of Medicine, 390, 1793–1801,https://doi.org/10.1056/NEJMra2210769, 2024.

Buschow, S., Keller, J., and Wahl, S.: Explaining heatwaves with machine learning, Quarterly Journal of the Royal Meteorological Society, 150, 1207–1221,https://doi.org/10.1002/qj.4642, 2024.

Cai, W., Zhang, C., Suen, H. P., Ai, S., Bai, Y., Bao, J., Chen, B., Cheng, L., Cui, X., and Dai, H.: The 2020 China report of the Lancet Countdown on health and climate change, The Lancet Public Health, 6, e64–e81,https://doi.org/10.1016/S2468-2667(20)30256-5, 2021.

https://doi.org/10.5194/egusphere-2026-3287
Preprint. Discussion started: 24 June 2026

Chauhan, A., Smith, P. A., Rodrigues, F., Christensen, A., St. John, M., and Mariani, P.: Distribution and impacts of long-lasting marine heat waves on phytoplankton biomass, Frontiers in Marine Science, 10, 1177571,https://doi.org/10.3389/fmars.2023.1177571, 2023.

Dar, J. A. and Apurv, T.: Spatiotemporal characteristics and physical drivers of heatwaves in India, Geophysical Research Letters, 51, e2024GL109785,https://doi.org/10.1029/2024GL109785, 2024.

Enliang, G., Yongfang, W., and Yulong, B.: Assessing spatiotemporal variation of heat waves during 1961–2016 across mainland China, International Journal of Climatology, 40, 3036–3051,https://doi.org/10.1002/joc.6381, 2020.

Feng, X., Liu, D., Zhao, J., Si, W., and Fan, S.: Impact of climate change on farmers' crop production in China: a panel Ricardian analysis, Humanities and Social Sciences Communications, 12, 1–12,https://doi.org/10.1057/s41599-024-04287-5, 2025.

Gu, X., Jiang, Z., Guan, Y., Luo, M., Li, J., Wang, L., Zhang, X., Kong, D., and Wang, L.: Frequent land-ocean transboundary migration of tropical heatwaves under climate change, Nature Communications, 16, 3400,https://doi.org/10.1038/s41467-025-58586-9, 2025.

Guo, H., Bao, A., Ndayisaba, F., Liu, T., Jiapaer, G., El-Tantawi, A. M., and De Maeyer, P.: Space-time characterization of drought events and their impacts on vegetation in Central Asia, Journal of Hydrology, 564, 1165–1178,https://doi.org/10.1016/j.jhydrol.2018.07.081, 2018.

Happé, T., Wijnands, J., Fernández-Torres, M. Á., Scussolini, P., Muntjewerf, L., and Coumou, D.: Detecting Spatiotemporal Dynamics of Western European Heatwaves Using Deep Learning, Artificial Intelligence for the Earth Systems, 3, e230107,https://doi.org/10.1175/AIES-D-23-0107.1, 2024.

Hobday, A. J., Alexander, L. V., Perkins, S. E., Smale, D. A., Straub, S. C., Oliver, E. C., Benthuysen, J. A., Burrows, M. T., Donat, M. G., and Feng, M.: A hierarchical approach to defining marine heatwaves, Progress in oceanography, 141, 227–238,https://doi.org/10.1016/j.pocean.2015.12.014, 2016.

Horowitz, R. L., McKinnon, K. A., and Simpson, I. R.: Circulation and soil moisture contributions to heatwaves in the United States, Journal of Climate, 35, 8031–8048,https://doi.org/10.1175/JCLI-D-21-0156.1, 2022.

Hu, Y., Jia, G., Gao, H., Li, Y., Hou, M., Li, J., and Miao, C.: Spatial characterization of global heat waves using satellite-based land surface temperature, International Journal of Applied Earth Observation and Geoinformation, 125, 103604,https://doi.org/10.1016/j.jag.2023.103604, 2023.

Jiang, L., Yang, Y., Wu, Q., Yang, L., and Yang, Z.: Hotter days, dirtier air: the impact of extreme heat on energy and pollution intensity in China, Energy Economics, 130, 107291,https://doi.org/10.1016/j.eneco.2023.107291, 2024.

Li, J., Zhang, Y., Yang, L., and Shan, Z.: Seasonal variations in ecological environment quality across different geomorphological regions and their response mechanisms to climate change, Scientific Reports, 15, 26385,https://doi.org/10.1038/s41598-025-11442-8, 2025.

Li, L., Zhang, Y., Liu, Q., Ding, M., and Mondal, P. P.: Regional differences in shifts of temperature trends across China between 1980 and 2017, Int. J. Climatol, 39, 1157–1165,https://doi.org/10.1002/joc.5868, 2019.

Luo, M., Lau, N.-C., and Liu, Z.: Different mechanisms for daytime, nighttime, and compound heatwaves in southern China, Weather and Climate Extremes, 36, 100449,https://doi.org/10.1016/j.wace.2022.100449, 2022a.

Luo, M., Lau, N. C., Liu, Z., Wu, S., and Wang, X.: An observational investigation of spatiotemporally contiguous heatwaves in China from a 3D perspective, Geophysical Research Letters, 49, e2022GL097714,https://doi.org/10.1029/2022GL097714, 2022b.

Luo, M., Wang, X., Dong, N., Zhang, W., Li, J., Wu, S., Ning, G., Dai, L., and Liu, Z.: Two different propagation patterns of spatiotemporally contiguous heatwaves in China, Npj Climate and Atmospheric Science, 5, 89,https://doi.org/10.1038/s41612-022-00313-y, 2022c.

Luo, M., Wu, S., Lau, G. N.-C., Pei, T., Liu, Z., Wang, X., Ning, G., Chan, T. O., Yang, Y., and Zhang, W.: Anthropogenic forcing has increased the risk of longer-traveling and slower-moving large contiguous heatwaves, Science Advances, 10, eadl1598,https://doi.org/10.1126/sciadv.adl1598, 2024.

Lyu, J., Shi, Y., Liu, T., Xu, X., Liu, S., Yang, G., Peng, D., Qu, Y., Zhang, S., and Chen, C.: Extreme drought-heatwave events threaten the biodiversity and stability of aquatic plankton communities in the Yangtze River ecosystems, Communications Earth & Environment, 6, 171,https://doi.org/10.1038/s43247-025-02143-1, 2025.

https://doi.org/10.5194/egusphere-2026-3287
Preprint. Discussion started: 24 June 2026

Marengo, J. A., Costa, M. C., Cunha, A. P., Espinoza, J.-C., Jimenez, J. C., Libonati, R., Miranda, V., Trigo, I. F., Sierra, J. P., and Geirinhas, J. L.: Climatological patterns of heatwaves during winter and spring 2023 and trends for the period 1979–2023 in central South America, Frontiers in Climate, 7, 1529082,https://doi.org/10.3389/fclim.2025.1529082, 2025.

Martinez-Villalobos, C., Fu, D., Loikith, P. C., and Neelin, J. D.: Accelerating increase in the duration of heatwaves under global warming, Nature Geoscience, 18, 716–723,https://doi.org/10.1038/s41561-025-01737-w, 2025.

Muñoz-Sabater, J., Dutra, E., Agustí-Panareda, A., Albergel, C., Arduini, G., Balsamo, G., Boussetta, S., Choulga, M., Harrigan, S., and Hersbach, H.: ERA5-Land: A state-of-the-art global reanalysis dataset for land applications, Earth system science data, 13, 4349–4383,https://doi.org/10.5194/essd-13-4349-2021, 2021.

Perkins-Kirkpatrick, S. and Lewis, S.: Increasing trends in regional heatwaves, Nature communications, 11, 3357, 2020.

Qiao, Z., Wang, N., Chen, J., Xu, X., Liu, L., and Han, D.: Understanding the differences in the contribution and impact of urbanization on urban warming during heatwave and non-heatwave periods in China, Journal of Cleaner Production, 474, 143626,https://doi.org/10.1016/j.jclepro.2024.143626, 2024.

Qiu, W. and Yan, X.: The trend of heatwave events in the Northern Hemisphere, Physics and Chemistry of the Earth, Parts A/B/C, 116, 102855,https://doi.org/10.1016/j.pce.2020.102855, 2020.

Ren, J., Wang, C., and Yao, Y.: Spatiotemporally continuous marine heatwaves: A novel clustering approach reveals increasing frequency, duration, area, intensity, and movement distance, Geophysical Research Letters, 52, e2024GL113211,https://doi.org/10.1029/2024GL113211, 2025.

Sánchez-Benítez, A., Barriopedro, D., and García-Herrera, R.: Tracking Iberian heatwaves from a new perspective, Weather and Climate Extremes, 28, 100238,https://doi.org/10.1016/j.wace.2019.100238, 2020.

Sánchez-Benítez, A., García-Herrera, R., Barriopedro, D., Sousa, P. M., and Trigo, R. M.: June 2017: The earliest European summer mega-heatwave of reanalysis period, Geophys Res Lett, 45, 1955–1962,https://doi.org/10.1002/2018GL077253, 2018.

Shi, P., Li, Y., Biswas, A., Wei, K., and Hou, M.: Spatial-temporal evolution and intrinsic drivers of compound drought and heatwave events in Mainland China, Science of the Total Environment, 948, 174834,https://doi.org/10.1016/j.scitotenv.2024.174834, 2024a.

Shi, T., Liu, W., Li, X., Zhang, T., Qiao, S., Yu, W., Xu, L., and Deng, K.: Comparative Analysis of the 2013 and 2022 Record-Breaking Heatwaves over the Yangtze River Basin, Ocean-Land-Atmosphere Research, 3, 0071,https://doi.org/10.34133/olar.0071, 2024b.

Skinner, C. B., Touma, D., Barlow, M., Singh, D., and King, T.: The spatial extent of heat waves has changed over the past four decades, Communications Earth & Environment, 6, 662,https://doi.org/10.1038/s43247-025-02661-y, 2025.

Sun, Z., Chen, C., Yan, M., Shi, W., Wang, J., Ban, J., Sun, Q., He, M. Z., and Li, T.: Heat wave characteristics, mortality and effect modification by temperature zones: a time-series study in 130 counties of China, International journal of epidemiology, 49, 1813–1822,https://doi.org/10.1093/ije/dyaa104, 2020.

Tan, Z., Liu, Y., Li, D., Tang, W., Gao, J., and Dong, X.: Impacts of massive topographies on heat waves in global drylands, Geophysical Research Letters, 51, e2024GL109979,https://doi.org/10.1029/2024GL109979, 2024.

Tian, Y., Guo, H., Guo, C., Li, B., Cao, Y., Jiang, L., Bao, A., and De Maeyer, P.: Event-based evaluation of IMERG for extreme precipitation in China: Insights from an error decomposition approach, Journal of Hydrology: Regional Studies, 61, 102657,https://doi.org/10.1016/j.ejrh.2025.102657, 2025.

Wang, A., Lettenmaier, D. P., and Sheffield, J.: Soil moisture drought in China, 1950–2006, Journal of Climate, 24, 3257–3271,https://doi.org/10.1175/2011JCLI3733.1, 2011.

Wang, C., Li, Z., Chen, Y., Li, Y., Ouyang, L., Zhu, J., Sun, F., Song, S., and Li, H.: Changes in global heatwave risk and its drivers over one century, Earth's Future, 12, e2024EF004430,https://doi.org/10.1029/2024EF004430, 2024a.

Wang, M., Huang, Y., Franzke, C. L., Yuan, N., Fu, Z., and Boers, N.: Evidence for preferred propagating terrestrial heatwave pathways due to Rossby wave activity, Nature Communications, 16, 4742,https://doi.org/10.1038/s41467-025-60104-w, 2025.

Wang, X., Zhang, Z., Yu, E., Guo, C., Otterå, O. H., and Counillon, F.: Warm advection as a cause for extreme heat event in North China, Geophysical Research Letters, 51, e2024GL108995,https://doi.org/10.1029/2024GL108995, 2024b.

Wei, J., Wang, W., Wang, G., Cao, M., Yang, L., Zhang, S., Fu, J., and Xing, W.: Projecting the changes in multifaceted characteristics of heatwave events across China, Earth's Future, 11, e2022EF003387,https://doi.org/10.1029/2022EF003387, 2023.

https://doi.org/10.5194/egusphere-2026-3287
Preprint. Discussion started: 24 June 2026

White, R. H., Anderson, S., Booth, J. F., Braich, G., Draeger, C., Fei, C., Harley, C. D., Henderson, S. B., Jakob, M., and Lau, C.-A.: The unprecedented Pacific northwest heatwave of June 2021, Nature communications, 14, 727,https://doi.org/10.1038/s41467-023-36289-3, 2023.

Wu, X., Wang, J., Ge, Y., Lai, S., Zhang, D., Ren, Z., and Wang, J.: Future heat-related mortality in Europe driven by compound day-night heatwaves and demographic shifts, Nature Communications, 16, 7420,https://doi.org/10.1038/s41467-025-62871-y, 2025.

Xu, K., Yang, D., Yang, H., Li, Z., Qin, Y., and Shen, Y.: Spatio-temporal variation of drought in China during 1961–2012: A climatic perspective, Journal of Hydrology, 526, 253–264,https://doi.org/10.1016/j.jhydrol.2014.09.047, 2015.

Xu, W., Yuan, W., Wu, D., Zhang, Y., Shen, R., Xia, X., Ciais, P., and Liu, J.: Impacts of record-breaking compound heatwave and drought events in 2022 China on vegetation growth, Agricultural and Forest Meteorology, 344, 109799,https://doi.org/10.1016/j.agrformet.2023.109799, 2024.

Yang, Q., Peng, H., and Li, Q.: Study on urban heatwave characteristics and thermal stress scenarios based on China's heatwave hazard zoning, Urban Climate, 55, 101957,https://doi.org/10.1016/j.uclim.2024.101957, 2024.

Yao, R., Hu, Y., Sun, P., Bian, Y., Liu, R., and Zhang, S.: Effects of urbanization on heat waves based on the wet-bulb temperature in the Yangtze River Delta urban agglomeration, China, Urban Climate, 41, 101067,https://doi.org/10.1016/j.uclim.2021.101067, 2022.

Yilmaz, M.: Accuracy assessment of temperature trends from ERA5 and ERA5-Land, Science of the Total Environment, 856, 159182,https://doi.org/10.1016/j.scitotenv.2022.159182, 2023.

Yu, Y., Shao, Q., Lin, Z., and Kang, I. S.: Characteristics analysis and synoptic features of event-based regional heatwaves over China, Journal of Geophysical Research: Atmospheres, 126, e2020JD033865,https://doi.org/10.1029/2020JD033865, 2021.

Zhang, B., He, Y., Wang, Z., Huang, B., Xie, Y., Guan, X., and Huang, J.: Disagreement in detected heatwave trends resulting from diagnostic methods, Geophysical Research Letters, 52, e2024GL114398,https://doi.org/10.1029/2024GL114398, 2025.

Zhao, P., He, Z., Ma, D., and Wang, W.: Evaluation of ERA5-Land reanalysis datasets for extreme temperatures in the Qilian Mountains of China, Frontiers in Ecology and Evolution, 11, 1135895,https://doi.org/10.3389/fevo.2023.1135895, 2023.

Zhou, Z., Guo, Y., Chen, D., Li, K., Wang, R., Wei, X., Zhang, J., Zhao, C., Tong, Z., and Liu, X.: Identification and spatiotemporal characteristic analysis of compound weather and climate extremes for maize in different climate zones of the Songliao Plain, International Journal of Disaster Risk Science, 15, 831–851,https://doi.org/10.1007/s13753-024-00585-3, 2024.

Zou, J., Lu, N., Jiang, H., Qin, J., Yao, L., Xin, Y., and Su, F.: Performance of air temperature from ERA5-Land reanalysis in coastal urban agglomeration of Southeast China, Science of The Total Environment, 828, 154459,https://doi.org/10.1016/j.scitotenv.2022.154459, 2022.